A Continuous Multicomponent Fuel Flame Propagation and Chemical Kinetics Model

Shiyou Yang

Rolf D. Reitz

Engine Research Center,
University of Wisconsin-Madison,
1500 Engineering Drive,
Madison, WI 53706

A continuous multicomponent fuel flame propagation and chemical kinetics model has been developed. In the multicomponent fuel model, the theory of continuous thermodynamics was used to model the properties and composition of fuels such as gasoline. The difference between the current continuous multicomponent fuel model and previous similar models in the literature is that the source terms contributed by chemistry in the mean and the second moment transport equations have been considered. This new model was validated using results from a discrete multicomponent fuel model. In the flame propagation and chemical kinetics model, five improved combustion submodels were also integrated with the new continuous multicomponent fuel model. To consider the change in local fuel vapor mixture composition, a "primary reference fuel (PRF) adaptive" method is proposed that formulates a relationship between the fuel vapor mixture PRF number (or research octane number) and the fuel vapor mixture composition based on the mean molecular weight and/or variance of the fuel vapor mixture composition in each cell. Simulations of single droplet vaporization with a single-component fuel (iso-octane) were compared with multicomponent fuel cases. [DOI: 10.1115/1.4000267]

Keywords: continuous multicomponent fuel model, flame propagation, G-equation, detailed chemical kinetics

1 Introduction

For simplicity, fuels are often represented as a single-component fuel in most multidimensional models, such as the KIVA code [1]. However, single-component fuel models are not able to predict the complex behavior of the vaporization of multicomponent fuels such as gasoline and diesel. The preferential vaporization of light-end components in multicomponent fuels affects greatly the fuel distribution near the spray and cannot be represented by single-component models [2]. Multicomponent fuel models are classified into two types, i.e., discrete multicomponent (DMC) models and continuous multicomponent (CMC) models. The discrete component approach has high computational overhead when it is used for fuels with a large number of components, because additional transport equations are to be solved for each species in order to track the fuel composition and the vaporization behavior. The CMC model, which is based on the continuous thermodynamics method [3], represents the fuel composition as a continuous distribution function with respect to an appropriate parameter, such as molecular weight. This enables a reduction in computational load without degrading the predictability of the complex behavior of the vaporization of multicomponent fuels [2]. The continuous multicomponent (CMC) model was first implemented into the engine simulation KIVA code to simulate realistic fuel spray and evaporation by Lippert and Reitz [4].

In order to avoid overprediction or underprediction of the evaporation mass flux depending on the ambient temperature conditions, Ra and Reitz [5] added a submodel into the continuous multicomponent KIVA code in which the droplet surface temperature (which is not necessarily equal to the droplet average temperature) could be separately calculated. However, in the works in Refs. [2–5], only the effects of multicomponent fuels on spray and evaporation were considered. In the combustion model the fuel was still considered as a single-component fuel.

The turbulent ignition and combustion process in spark ignition (SI) engines is a complicated aerothermochemical process, especially due to the turbulence and chemistry interactions that occur on tremendously different time-scale and length-scale levels. The level-set method (G-equation) is a powerful tool to model both premixed and partially premixed combustion occurring in SI engines. With its application to combustion, Williams [6] first suggested the use of a transport equation for a nonreactive scalar, G, for laminar flame propagation. Peters [7] subsequently extended this approach to the turbulent flame regime. The turbulent G-equation concept has been successfully applied to SI engine combustion simulations by Tan [8].

A large amount of work has been done on developing detailed chemical kinetics mechanisms for fuel oxidation and pollutant formation [9]. Liang [10] successfully incorporated detailed chemical kinetics into a G-equation-based turbulent combustion model, which was implemented into the KIVA-3V release 2 code by Tan [8]. In the G-equation-based turbulent combustion model the laminar flame speed is very important for determining the propagation of the flame front ($G=0$) surface. Also, the local and instantaneous residual value has a great effect on the evaluation of the laminar flame speed. For the calculation of the residual value, Yang et al. [11] used several different empirical methods, in which several improvements to the G-equation combustion submodels were proposed. Yang et al. [12] subsequently proposed a transport equation residual model incorporating a Damkohler criterion for accurately calculating the local and instantaneous residual in each cell and fundamentally describing the combustion process in the flame-containing cells.

However, in the works in Refs. [8,10–12], the fuel was assumed to be a single-component fuel. A continuous multicomponent fuel evaporation model was integrated with an improved G-equation combustion and detailed chemical kinetics model by Yang and Reitz [13]. However, the source terms contributed by chemistry in the mean and the second moment transport equations were not

Contributed by the IC Engine Division of ASME for publication in the JOURNAL OF ENGINEERING FOR GAS TURBINES AND POWER. Manuscript received April 30, 2009; final manuscript received August 29, 2009; published online April 14, 2010. Assoc. Editor: James S. Wallace.

considered, and in the calculation of laminar flame speed only the average primary reference fuel (PRF) number was used.

In this paper, we develop a continuous multicomponent fuel flame propagation and chemical kinetics model. In this model the source terms contributed by chemistry in the mean and the second moment transport equations are considered. This new model is validated with a constant volume combustion case. In the flame propagation and chemical kinetics model, five improved combustion submodels previously developed are integrated with the new continuous multicomponent fuel model.

2 Models

2.1 CMC Fuel Model. Consider a spherical liquid droplet with a large number of components vaporizing in a gaseous environment. The governing equations for the vapor phase fuel, the liquid phase fuel, along with the liquid-vapor equilibrium at the interface between the droplet and surrounding gas, are considered next.

2.1.1 Vapor Phase Transport Equations. Based on the continuous thermodynamics approach, the governing equations for the various moments of the fuel vapor distribution in the gas phase can be derived. For the two-parameter-type Γ distribution function used in this paper, three equations suffice for the calculations. The governing equations for the continuity, mean molecular weight θ, and the second moment of the fuel vapor distribution Ψ have been derived in Refs. [5,13]. In those equations only source terms from the fuel spray, $d/dt(\rho y_F)^s$, $d/dt(\rho y_F\theta)^s$, and $d/dt(\rho y_F\Psi)^s$ are considered, which are obtained from the liquid phase calculation and the exchange between the liquid phase and the vapor phase. However, in combustion application such as gasoline engines, in the unburned region in front of flame front, chemical kinetics must be considered as it is important for knock. The different chemical kinetics rates of the fuel species may also contribute to the source terms of y_F, θ, and Ψ. Considering the source terms contributed by either chemical kinetics or equilibrium chemistry, the governing equations for the continuity, mean molecular weight θ, and the second moment of the fuel vapor distribution Ψ are

$$\frac{\partial}{\partial t}(\rho y_F) + \nabla\cdot(\rho\vec{\mathbf{v}}y_F) = \nabla\cdot(\rho\bar{D}\,\nabla\, y_F) + \frac{d}{dt}(\rho y_F)^s + \frac{d}{dt}(\rho y_F)^c \tag{1}$$

$$\frac{\partial}{\partial t}(\rho y_F\theta) + \nabla\cdot(\rho\vec{\mathbf{v}}y_F\theta) = \nabla\cdot(\rho\tilde{D}\,\nabla\,(y_F\theta)) + \frac{d}{dt}(\rho y_F\theta)^s + \frac{d}{dt}(\rho y_F\theta)^c \tag{2}$$

$$\frac{\partial}{\partial t}(\rho y_F\Psi) + \nabla\cdot(\rho\vec{\mathbf{v}}y_F\Psi) = \nabla\cdot(\rho\hat{D}\,\nabla\,(y_F\Psi)) + \frac{d}{dt}(\rho y_F\Psi)^s + \frac{d}{dt}(\rho y_F\Psi)^c \tag{3}$$

where ρ is the density of the gas mixture and y_F is the mass fraction of the continuous fuel vapor. $\vec{\mathbf{v}}$ is the mass-averaged velocity of the gas phase mixture. $\bar{D}$, $\tilde{D}$, and $\hat{D}$ are diffusion coefficients associated with the diffusion processes of the vapor mass, the vapor mean molecular weight, and the second moment of the vapor distribution, respectively. Since the values of these coefficients are very close to each other [3], they are assumed to be equal. The superscript c means the source terms are contributed by chemistry. The moments θ and Ψ are defined as

$$\theta = \int_0^\infty f(I)I\,dI \tag{4}$$

$$\Psi = \int_0^\infty f(I)I^2\,dI \tag{5}$$

where $f(I)$ is a distribution function or probability density function (PDF), and I is the mean molecular weight of the fuel. The energy equation can be derived and simplified as

$$\bar{C}_P\frac{\partial}{\partial t}(\rho T) + \bar{C}_P\,\nabla\cdot(\rho\vec{\mathbf{v}}T) = \nabla\cdot\lambda\,\nabla\,T + [(a_c - C_{PA})\rho\bar{D} + b_c\rho\theta\tilde{D}]\,\nabla\, y_F\cdot\nabla T \tag{6}$$

where $\bar{C}_P$ is the mixture specific heat, T is the temperature, λ is the thermal conductivity, C_{pA} is the specific heat of air, and a_c and b_c are the coefficients of a linear correlation of specific heat taken from Chou and Prausnitz [14] as a function of composition. The energy equation (6) is used for solving the droplet surface temperature, as described by Ra and Reitz [5].

The multicomponent fuel model described by Eqs. (1)–(3) is called "continuous multicomponent fuel chemistry model" in this paper, and the source terms are discussed later.

2.1.2 Liquid Phase Governing Equations. Assuming that there is no absorption of ambient gas into the liquid droplet, a general form of the governing equation for the change rate of the various moments of the liquid fuel distribution is [5]

$$\frac{\rho_L R}{3}\frac{d\theta_L^n}{dt} = \dot{m}\frac{\theta_L^1}{\theta_V^1}(\theta_L^n - \theta_V^n) \quad (n = 1,2,\ldots) \tag{7}$$

where ρ_L is the mass density of the liquid fuel, R is the droplet radius, θ_L^n and θ_V^n are the nth moments of the fuel distribution in the liquid phase and vapor phase, respectively, as defined in Eqs. (4) and (5), and $\dot{m}$ is the vaporization mass flux. Substituting $n=1$ and $n=2$ into Eq. (7), the governing equation for the change rate of the first and second moments of the liquid phase composition can be obtained as

$$\frac{d\theta_L}{dt} = \frac{3\dot{m}}{\rho_L R}\frac{\theta_L}{\theta_V}(\theta_L - \theta_V) \tag{8}$$

$$\frac{d\Psi_L}{dt} = \frac{3\dot{m}}{\rho_L R}\frac{\theta_L}{\theta_V}(\Psi_L - \Psi_V) \tag{9}$$

The vaporization mass flux $\dot{m}$ is closely coupled with the source terms in the vapor phase transport Eqs. (1)–(3). Ra and Reitz showed the calculation of $\dot{m}$ in detail in Ref. [5]. The source terms in the vapor phase transport equations (2) and (3) can be derived as

$$\theta^s = Y_{F,R}\theta_R - \frac{1}{B}(\theta_\infty Y_{F,\infty} - \theta_R Y_{F,R}) \tag{10}$$

$$\Psi^s = Y_{F,R}\Psi_R - \frac{1}{B}(\Psi_\infty Y_{F,\infty} - \Psi_R Y_{F,R}) \tag{11}$$

where $Y_{F,R}$ is the fuel vapor molar fraction at the droplet surface, θ_R and Ψ_R are the mean molecular weight and the second moment of the fuel vapor distribution at the droplet surface, $Y_{F,\infty}$ is the fuel vapor molar fraction at an infinite ambient, which can be approximated as the studied cell's value, θ_∞ and Ψ_∞ are the mean molecular weight and the second moment of the fuel vapor distribution in the studied cell, and B is the Spalding number, which is calculated as

$$B = (Y_{F,R} - Y_{F,\infty})/(1 - Y_{F,R}) \tag{12}$$

The calculation of $Y_{F,R}$, θ_R, and Ψ_R will be shown later.

2.1.3 Vapor-Liquid Equilibrium. In the continuous thermodynamics approach, the equilibrium at the interface between the liquid droplet and the surrounding gas is based on the assumption

that the chemical potential for the liquid phase and the vapor phase are equal for each value of I. The fuel vapor mole fraction at the droplet surface can be determined by using Raoult's law as

$$Y_{FR} = \frac{P_{\text{atm}}}{P} \frac{\exp[A(1-\gamma B)]}{(1+AB\beta_L)^{\alpha_L}} \tag{13}$$

where P_{atm} is the reference pressure of 101.325 kPa, P is the pressure, and A and B are functions of temperature from the integration of the composition-dependent Clausius–Clapeyron equation. The Clausius–Clapeyron equation is of the form:

$$P^{\text{sat}}(I) = P_{\text{atm}} \cdot \exp\left[\frac{s_{fg}}{\bar{R}}\left(1 - \frac{T_B(I)}{T}\right)\right] \tag{14}$$

where s_{fg} is the entropy of vaporization (which is expressed by using Trouton's law as $s_{fg} = IL_V/T_B \approx 10.6\bar{R} \approx 87.9$, L_V is the vapor latent heat of evaporation, and T_B is the normal boiling point temperature of component I), $\bar{R}$ is the universal gas constant, and T is the droplet temperature. Assuming a linear variation in the normal boiling point temperature with composition $T_B(I) = a_B + b_B I$, with a_B and b_B constants obtained from regression of boiling data for the particular homologous family of components ($a_B = 208.53$, $b_B = 1.5763$), the vapor pressure can be expressed as

$$P^{\text{sat}}(I) = P_{\text{atm}} \cdot \exp[A(1 - B \cdot I)] \tag{15}$$

In this study, A and B are expressed as

$$A = \frac{s_{fg}}{\bar{R}}\left(1 - \frac{208.53}{T}\right), \quad B = \frac{1.5763}{T - 208.53} \tag{16}$$

Using Eqs. (13)–(16), a simple relation between the distribution parameters in the liquid and vapor phases can be obtained as

$$\theta_V = \gamma + \frac{\theta_L - \gamma}{\left(1 + \dfrac{AB\sigma_L^2}{\theta_L - \gamma}\right)}, \quad \sigma_V^2 = \sigma_L^2\left[\frac{\theta_V - \gamma}{\theta_L - \gamma}\right]^2 \tag{17}$$

θ_V and σ_V^2 calculated from Eq. (17) are the values at the droplet surface, and they can be used to calculate Ψ_R.

2.2 *G*-Equation Flame Propagation and Chemical Kinetics Model. The G-equation combustion model is mainly based on the turbulent premixed combustion flamelet theory by Peters [7], where a set of Favre-averaged level-set equations was derived, including equations for the Favre mean, $\tilde{G}$, and its variance, $\tilde{G}''^2$, and a model equation for the turbulent/laminar flame surface area ratio σ_T, which, in turn, results in an explicit expression for the turbulent flame speed S_T^0. In G-equation combustion model G is a scalar variable, and its value is zero at the flame front surface. These equations, together with the Reynolds averaged Navier–Stokes equations and the turbulence modeling equations, form a complete set to describe premixed turbulent flame front propagation. The equation set suitable for implementation in computational fluid dynamics (CFD) codes is [10]

$$\frac{\partial \tilde{G}}{\partial t} + (\tilde{\vec{u}} - \vec{u}_{\text{vertex}}) \cdot \nabla \tilde{G} = \frac{\bar{\rho}_u}{\bar{\rho}} S_T^0 |\nabla \tilde{G}| - D_T \tilde{k} |\nabla \tilde{G}| \tag{18}$$

$$\frac{\partial \tilde{G}''^2}{\partial t} + \tilde{\vec{u}} \cdot \nabla \tilde{G}''^2 = \nabla_{\|} \cdot \left(\frac{\bar{\rho}_u}{\bar{\rho}} D_T \nabla_{\|} \tilde{G}''^2\right) + 2D_T (\nabla \tilde{G})^2 - c_s \frac{\tilde{\varepsilon}}{\tilde{k}} \tilde{G}''^2 \tag{19}$$

$$\frac{S_T^0}{S_L^0} = 1 + I_P \left\{ -\frac{a_4 b_3^2}{2b_1}\frac{l_I}{l_F} + \left[\left(\frac{a_4 b_3^2}{2b_1}\frac{l_I}{l_F}\right)^2 + a_4 b_3^2 \frac{u' l_I}{S_L^0 l_F}\right]^{1/2} \right\} \tag{20}$$

where $\tilde{\vec{u}}$ is the Favre-average fluid velocity, $\vec{u}_{\text{vertex}}$ is the mesh vertex velocity which accounts for mesh movement, $\nabla \tilde{G}$ is the gradient of $\tilde{G}$, $\nabla \tilde{G}''^2$ is the gradient of $\tilde{G}''^2$, $\bar{\rho}_u$ is the Reynolds-average of the unburned mixture density, $\bar{\rho}$ is the Reynolds-average of the cell gas density, S_T^0 is the turbulent flame speed, D_T is the turbulent diffusivity, $\nabla_{\|}$ denotes the tangential gradient operator, c_s is a modeling constant, $\tilde{k}$ and $\tilde{\varepsilon}$ are the Favre mean turbulent kinetic energy and its dissipation rate from the renormalization group (RNG) k-ε model [15], u' is the turbulence intensity, S_L^0 is the laminar flame speed, l_I and l_F are the turbulence integral length scale and the laminar flame thickness, respectively, and a_4, b_3, b_1 are constants from turbulent flame speed model [7]. The term I_P in Eq. (20), called a progress variable in Ref. [10], takes the form:

$$I_P = \left[1 - \exp\left(-c_{m2}\frac{t - t_0}{\tau}\right)\right]^{1/2} \tag{21}$$

where c_{m2} is a model constant, t_0 is the spark timing, and $\tau = \tilde{k}/\tilde{\varepsilon}$ is the turbulence time scale.

In our previous work [11–13], five improved combustion submodels were developed for modeling gasoline engines with the level-set G-equation and detailed chemical kinetics. These combustion submodels include a transport equation residual model, introduction of a Damkohler criterion model for assessing the combustion regime of flame-containing cells, precise calculation of "primary heat release" based on the subgrid scale unburned/burnt volumes of flame-containing cells, modeling flame front quenching in highly stratified mixtures, and a recently developed PRF mechanism.

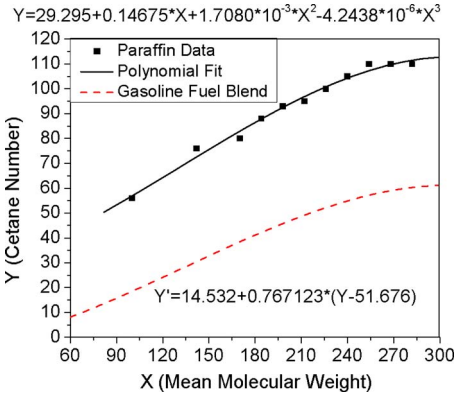

Fig. 1 Cetane number as a function of paraffin (alkane) molecular weight (after Rose and Cooper [16])

2.3 PRF-Adaptive Model for Integrating the CMC Fuel Model and the *G*-Equation Combustion Model. In the CMC fuel model described earlier, the fuel composition is represented by a PDF or distribution function. In the calculation the mean molecular weight (the first moment of the distribution function) θ, the second moment Ψ, and its variance σ^2 can be tracked. However, this composition representation is just an "abstract" composition representation. The actual quantity of each fuel species is needed in the combustion calculation after fuel evaporation. To track the "actual" fuel composition, a PRF-adaptive model is introduced in this paper. In this model, to consider the change in local fuel vapor mixture composition, a relationship between the fuel vapor mixture PRF number (or research octane number) and the fuel vapor mixture composition based on the mean molecular weight and/or variance of the fuel vapor mixture composition in each cell is formulated.

The cetane number (CN) has been measured for a variety of pure hydrocarbons [16]. Data for paraffins (alkanes) are shown in Fig. 1. The cetane number increases with molecular weight up to octadecane (MW=254.48, CN=110) after which no further in-

Table 1 Parameters for different fuels

Fuel	Gasoline	DF2 (diesel fuel no. 2)
Mean molecular weight (g/mol)	85.5	185.0
RON	95.4	29.0
CN	14.5	42.4
CN_{par}	51.7	88.0

crease is observed. These data were curve-fit with a third order polynomial (R^2=0.9878), which can be written as

$$CN_{par} = 29.295 + 0.14675 \times \theta + 1.7080 \times 10^{-3} \times \theta^2 - 4.2438 \times 10^{-6} \times \theta^3 \quad (22)$$

where θ represents the mean molecular weight of the vapor distribution.

The CN is evaluated based on the mean molecular weight of the computational cell composition distribution. It should be noted, however, that Eq. (22) cannot be used directly as a calculation of the cetane number in the computational cell because the gasoline fuel vapor exists as a blend of many components, which have not been taken into account explicitly. Hence, the cetane number was adjusted to account for the composition by means of a second correction, also shown in Fig. 1. Before the adjustment, a relation between the CN and the research octane number (RON), which was proposed by Kalghatgi [17], is introduced, viz.,

$$CN = 54.6 - 0.42 \times RON \quad (23)$$

In Kalghatgi's work [17], cetane numbers were measured for PRFs using the ASTM D613 (engine) method, and the measured cetane numbers were plotted against RON. For DF2 (diesel fuel no. 2) the PRF (RON) is 29, according to Eq. (23), the cetane number of DF2 is

$$CN = 54.6 - 0.42 \times 29 = 42.42. \quad (24)$$

Thus, a second correction can be constructed such that gasoline (MW=85.5) yields a CN of 14.532, and DF2 (diesel fuel no. 2 with MW=185.0) yields a CN of 42.42. This correlation is based on the data of Table 1, and can be expressed as

$$CN = 14.532 + 0.767123 \times (CN_{par} - 51.676) \quad (25)$$

Inserting Eq. (22) into Eq. (25) gives

$$CN = 14.532 + 0.767123 \times (-22.381 + 0.14675 \times \theta + 1.7080 \times 10^{-3} \times \theta^2 - 4.2438 \times 10^{-6} \times \theta^3)$$

and with Eq. (23) gives

$$RON = 136.279 - 0.268 \times \theta - 0.00312 \times \theta^2 + 0.00000775 \times \theta^3 \quad (26)$$

Equation (26) is a relationship between the fuel vapor mixture PRF number (or research octane number) and the fuel vapor mixture composition based on the mean molecular weight of the fuel vapor mixture composition in each cell. Equation (26) is shown in Fig. 2. Because the CMC model tracks the mean molecular weight (the first moment of the distribution function) θ of each cell, the octane number of the fuel vapor mixture can be calculated.

2.4 Continuous Multicomponent Fuel Chemistry Model. Now consider the chemistry source terms $d/dt(\rho y_F)^c$, $d/dt(\rho y_F\theta)^c$, and $d/dt(\rho y_F\Psi)^c$. In unburned regions, before calling chemical kinetics solver, the fuel is viewed as a multicomponent mixture. With the current mean molecular weight θ of the fuel vapor in the calculated cell, the PRF number can be calculated according to Eq. (26). With the calculated PRF number the fuel is divided into gasoline surrogate fuel "ic8h18" and diesel surrogate fuel "nc7h16" by corresponding fractions. Then the

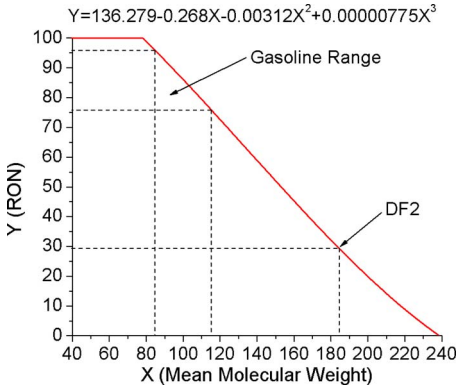

Fig. 2 RON as a function of computational cell fuel vapor mixture mean molecular weight

chemical kinetics solver provides the new ρ_{ic8h18}, ρ_{nc7h16} values, the two fuel species mole fractions Y_{ic8h18}, Y_{nc7h16}, and the mass density change rates of the two fuel species $d/dt(\rho y_{ic8h18})^c$, $d/dt(\rho y_{nc7h16})^c$ can be calculated. After calling the chemical kinetics solver, the mass density change rate of the multicomponent fuel is

$$\frac{d}{dt}(\rho y_F)^c = \frac{d}{dt}(\rho y_{ic8h18})^c + \frac{d}{dt}(\rho y_{nc7h16})^c \quad (27)$$

With the new mole fractions of the two fuel species Y_{ic8h18}, Y_{nc7h16}, the updated PRF number of the studied cell can be obtained and with Eq. (26), the updated θ^c can be calculated. The calculation of the updated Ψ^c is

$$\Psi^c = (\theta^c)^2 + (\alpha + 1) \times \beta^2 \quad (28)$$

In the burnt regions, the calculation process is the same as in the unburned regions, as described above.

In flame-containing cells, the chemistry source terms $d/dt(\rho y_F)^{ceq}$, $d/dt(\rho y_F\theta)^{ceq}$, and $d/dt(\rho y_F\Psi)^{ceq}$ are calculated as follows. Assume that in time step dt the flame propagates through the total V_u volume, then the end density of species k is $\rho y_{k,b}$, where ρ is the cell density and $y_{k,b}$ is the mass fraction of each species in the burnt and swept equilibrium region (Fig. 3). Assuming the initial density is ρ_{k0}, the density change rate of species k is

$$\frac{d\rho_k}{dt} = \frac{\rho y_{k,b} - \rho_{k0}}{dt} \quad (29)$$

But this density change rate corresponds to the volume V_u. If the actual volume V_s is swept, then the density change rate should be

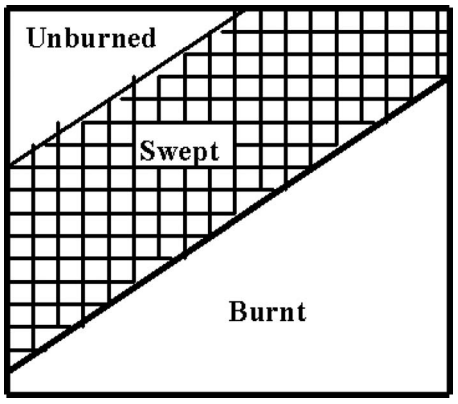

Fig. 3 Subgrid scale unburned/burnt regions

Table 2 Fuel distribution parameters

Fuel	Gasoline	Iso-octane
α	5.7	100
β	15	0.1
γ	0	104.2
θ	85.5	114.2
σ	35.8	1

$$\frac{d\rho_k}{dt} = \left(\frac{\rho y_{k,b} - \rho_{k0}}{dt}\right)\frac{V_s}{V_u} \tag{30}$$

With the current mean molecular weight θ of the fuel vapor in the calculated cell, the PRF number can be calculated according to Eq. (26). With the calculated PRF number the fuel is again divided into ic8h18 and nc7h16 with corresponding fractions. Then the chemistry equilibrium solver provides the updated $\rho y_{k,b}$ value of each species, and the two fuel species mole fractions Y_{ic8h18}, Y_{nc7h16}. After calling the chemistry equilibrium solver, the mass density of the multicomponent fuel is

$$(\rho y_{F,b})^{\text{ceq}} = (\rho y_{\text{ic8h18},b})^{\text{ceq}} + (\rho y_{\text{nc7h16},b})^{\text{ceq}} \tag{31}$$

The calculation of updated θ^{ceq} is as follows. With the new mole fractions of the two fuel species Y_{ic8h18}, Y_{nc7h16}, the updated PRF number can be calculated; with Eq. (26), the updated θ^{ceq} can be calculated. As in Eq. (28) the calculation of the updated Ψ^{ceq} is

$$\Psi^{\text{ceq}} = (\theta^{\text{ceq}})^2 + (\alpha + 1) \times \beta^2 \tag{32}$$

3 Results and Discussion

3.1 Results From the CMC Fuel Evaporation Model. The continuous multicomponent fuel evaporation model was first applied to study single stagnant droplet evaporation. In the simulation of an evaporating single droplet, the parameters of the Γ distribution function were chosen as shown in Table 2 for the composition of gasoline and iso-octane in the multicomponent fuel model. In the simulation the radiation is not included.

The simulation results for normal evaporation of gasoline droplets are shown in Figs. 4(*a*)–4(*c*). The initial ambient temperature and pressure are 1000 K and 1.0 bar, respectively, and the initial temperature and size of the droplet are 300 K and 100 μm, respectively. Because of preferential vaporization of the highly volatile light-end components in the gasoline composition, the mean molecular weight of the composition increases and the variance decreases steadily. The mass fraction of fuel vapor at the droplet surface decreases initially due to the increase in the mean of composition and the decrease in the surface temperature; it then increases because the heating effect is more than the reducing effect of the increase in the mean of composition.

Figure 5 shows a comparison of the predicted history of the droplet interior temperatures for gasoline and iso-octane droplets at ambient air pressures of 0.3 bar and 1.0 bar. The ambient temperature is 500 K, the initial droplet temperature is 300 K, and the initial droplet diameter is 100 μm. The gasoline droplet at the ambient pressure of 0.3 bar is vaporized through flash boiling initially [5] and the other cases are in the normal evaporation mode. The gasoline droplets initially experience a cooling process, while the iso-octane droplets are heated up from the beginning [5]. Figure 5 also shows an interesting characteristic of multicomponent fuel vaporization: Gasoline droplets do not reach an equilibrium temperature as in the case of the single-component iso-octane droplet, because the composition of the droplets is continuously changing as the more volatile components are vaporized.

Figure 6 shows the comparison of surface regression profiles for two ambient temperatures for gasoline and iso-octane droplets: 500 K and 1000 K. The ambient pressure is 1.0 bar, the initial droplet temperature is 300 K, and the initial droplet diameter is 100 μm. From Fig. 6, it is seen that as the ambient temperature increases the life time of the droplet decreases. Because the highly volatile light-end components in the gasoline composition evaporate preferentially, the gasoline droplet size decreases rapidly in the initial stage. However, compared with iso-octane the evaporation rate of gasoline slows down during the later stages.

Figure 7 shows the corresponding evolutions of droplet interior temperature and surface temperature for gasoline and iso-octane droplets. For iso-octane, initially the surface temperature is higher than the interior temperature, and then there is an equilibrium drop temperature at which the interior and surface temperatures of the drop become equal when no heat transfer between the interior

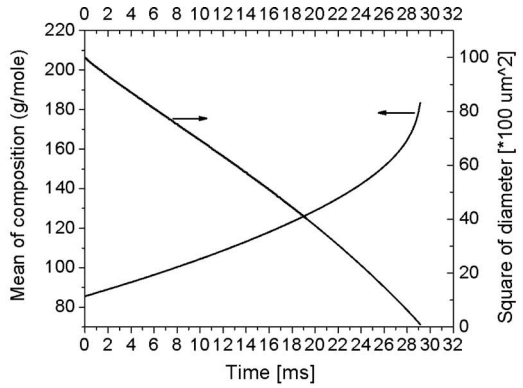

(a) Mean of composition and square of diameter of droplet

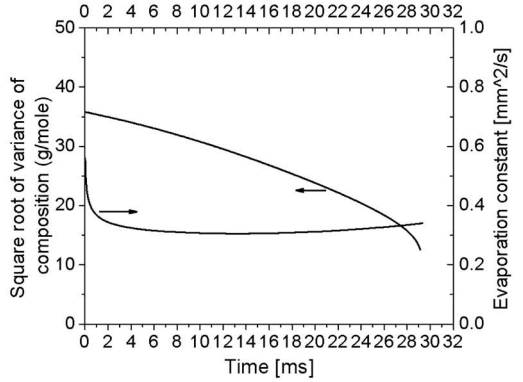

(b) Square root of variance and the evaporation constant

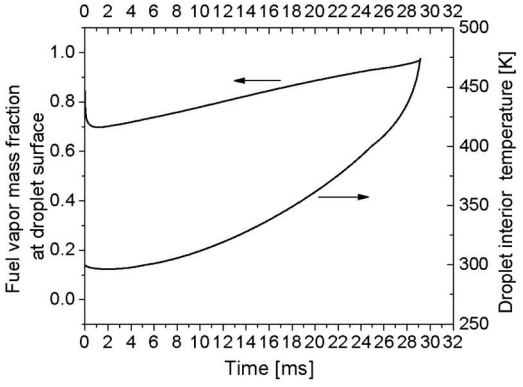

(c) Droplet surface fuel mass fraction and interior temperature

Fig. 4 Evaporation of a stagnant gasoline droplet in quiescent ambient air. (*a*) Mean of composition and square of diameter of droplet, (*b*) square root of variance and the evaporation constant, and (*c*) droplet surface fuel mass fraction and interior temperature.

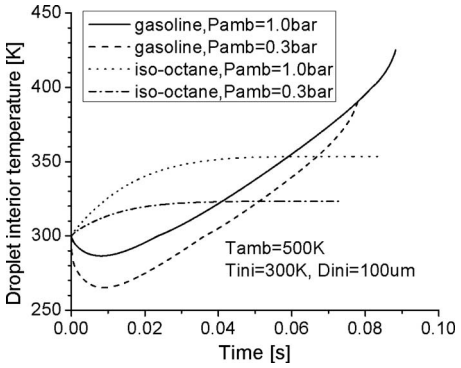

Fig. 5 Predicted history of the droplet interior temperature for gasoline and iso-octane droplets

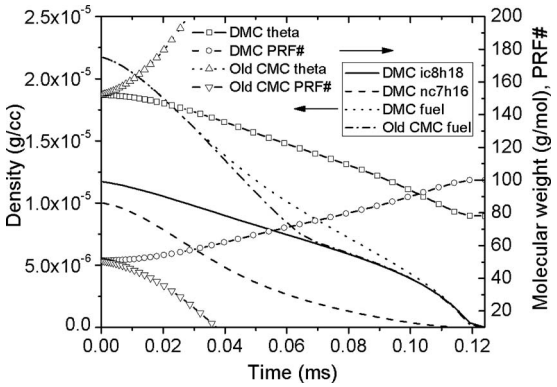

Fig. 8 Comparison between DMC and "old CMC"

and the surface of the drop occurs. For gasoline, because of the evaporation at the surface, the cooling process of the surface is more obvious than the droplet interior, so the initial surface temperature is lower than the interior temperature. Then, as it is heated up by the ambient gas, the surface temperature is higher than the interior temperature. Finally, the surface temperature is equal to the interior temperature. However, as mentioned above, the gasoline droplet does not reach an equilibrium temperature.

3.2 Validation of the CMC Fuel Chemistry Model. To validate the present continuous multicomponent fuel chemistry model, a constant volume computational region filled with 50–50% (in mole fraction) iso-octane/*n*-heptane and air mixture with overall equivalence ratio unity was studied. In the two-dimensional computation mesh, the bore is 12.664 cm, and there are 5000 cells. The initial pressure is 1.434 bar, and the initial temperature is 1500 K. Three different models were considered. The first model is the discrete multicomponent fuel model, the second model is the continuous multicomponent fuel model without considering the chemistry source terms "old CMC model," and the third model is the present continuous multicomponent fuel model that considers chemistry source terms "new CMC model." The results from the discrete multicomponent fuel model show that since *n*-heptane burns fast its mole fraction decreases while iso-octane's mole fraction increases as time increases, and thus the PRF number increases. According to Fig. 2, the fuel mean molecular weight decreases. Figure 8 shows the comparison between DMC and the old CMC. The variation in fuel PRF number and mean molecular weight are included in Fig. 8. Figure 8 also includes the density variation in iso-octane and *n*-heptane. It is seen that the fuel mean molecular weight and PRF number of the old CMC are totally different from those of DMC, which can be viewed as accurate solutions. For the old CMC model, $d/dt(\rho y_F \theta)^c$ and $d/dt(\rho y_F \Psi)^c$ in Eqs. (2) and (3) are not considered. In this simulation case, there is no spray source term, the gas is homogeneous, and there is no moving boundary, so the diffusion term and convection term in Eq. (2) are zero, and thus the equation becomes $\partial/\partial t(\rho y_F \theta)=0 \Rightarrow \rho_F \theta = \text{const} \Rightarrow$ as ρ_F decreases, θ increases. As θ increases, the fuel PRF number decreases. In Fig. 8, the fuel amount of old CMC also does not match the DMC result.

Figure 9 shows the comparison between the DMC and the new CMC models. From Fig. 9, it is seen that every parameter including fuel amount, fuel mean molecular weight and fuel PRF number from the new CMC is fairly close to that of the DMC model. So it is concluded that the proposed continuous multicomponent fuel chemistry model gives reasonable results.

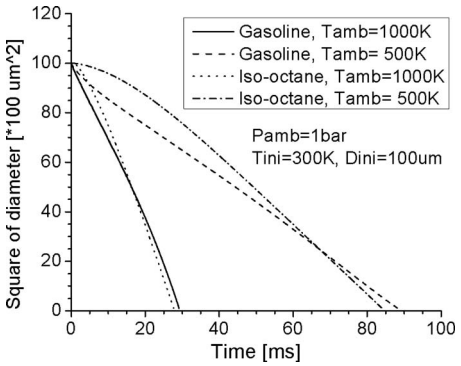

Fig. 6 Comparison of surface regression profiles for gasoline and iso-octane at two ambient temperatures

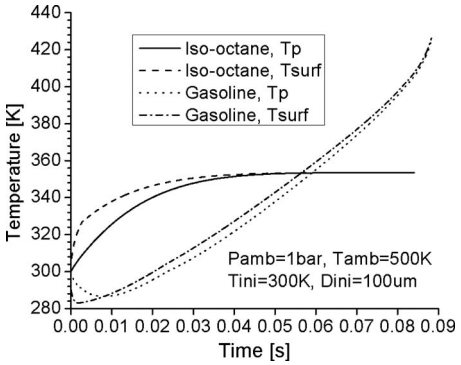

Fig. 7 Comparison of profiles of droplet interior temperature and surface temperature of iso-octane and gasoline vaporization

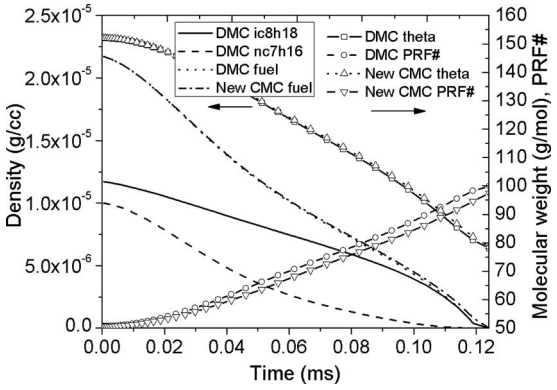

Fig. 9 Comparison between DMC and "new CMC"

4 Conclusions

In this study a continuous multicomponent fuel flame propagation and chemical kinetics model has been developed. The difference between the current continuous multicomponent fuel model and previous similar models in the literature is that the source terms contributed by chemistry in the mean and the second moment transport equations have been considered. In the flame propagation and chemical kinetics model, five improved combustion submodels previously developed were also integrated with the new continuous multicomponent fuel model. Based on the results, the following conclusions can be drawn.

1. Multicomponent fuels such as gasoline obviously have different vaporization characteristics from single component fuels such as iso-octane in that the vapor fuel distributions of their sprays are quite different. Therefore a multicomponent fuel model is necessary for more accurate predictions of the fuel distribution in the engine cylinder. The present CMC fuel model captures important multicomponent fuel characteristics, and saves computing time compared with DMC fuel models, since only two additional transport equations are needed.
2. The fuel composition of the new model proposed in this paper in combustion cases agrees well with that of the discrete multicomponent fuel model, which can be viewed as an accurate solution. The old model gives incorrect fuel composition results when it is used for a constant volume combustion case. This confirms the importance of accounting for chemistry effects in multicomponent fuel combustion modeling.
3. The proposed "PRF-adaptive" method allows integration of the continuous CMC fuel model and the *G*-equation combustion model.

Acknowledgment

This work was supported by Ford Research and Advanced Engineering. The authors thank Dr. Youngchul Ra and Dr. Long Liang for their helpful discussions and comments. Ford Research and Advanced Engineering is thanked for providing experimental test data.

Nomenclature

f = distribution function
I = species molecular weight
θ = mean molecular weight of fuel
Ψ = the second moment
ρ = mass density
y = mass fraction
$\vec{\mathbf{v}}$ = velocity
D = diffusion coefficient
C, c = specific heat
T = temperature
λ = thermal conductivity
R = droplet radius, universal gas constant
$\dot{m}$ = vaporization mass flux
Y = mole fraction
B = Spalding number
α, β, γ = parameters for distribution function
σ^2 = variance
P = pressure
s = entropy
S = flame speed
$\tilde{k}$ = Favre mean turbulent kinetic energy
$\tilde{\varepsilon}$ = dissipation rate
τ = turbulence time scale
ϕ = equivalence ratio

Subscripts and Superscripts

s = source term from spray, droplet surface, swept
F, f = fuel
P = constant pressure
v = constant volume
A = air
c = source term from chemistry
L = liquid, laminar
n = nth moment
V = vapor
R = droplet surface
∞ = infinite ambient
B, b = boiling point, burned mixture
d = droplet
u = unburned mixture
T = turbulent
par = paraffins

References

[1] Amsden, A. A., 1999, "KIVA-3V, Release 2, Improvements to KIVA-3V," Los Alamos National Laboratory Report No. LA-13608-MS.
[2] Lippert, A. M., 1999, "Modeling of Multi-Component Fuels with Application to Sprays and Simulation of Diesel Engine Cold Start," Ph.D. thesis, University of Wisconsin-Madison, Madison, WI.
[3] Tamim, J., and Hallett, W. L. H., 1995, "Continuous Thermodynamics Model for Multi-Component Vaporization," Chem. Eng. Sci., **50**(18), pp. 2933–2942.
[4] A. M. Lippert and R. D. Reitz, 1997, "Modeling of Multi-Component Fuels Using Continuous Distributions With Application to Droplet Evaporation and Sprays," SAE Paper No. 972882.
[5] Ra, Y., and Reitz, R. D., 2003, "The Application of a Multi-Component Droplet Vaporization Model to Gasoline Direct Injection Engines," Int. J. Engine Res., **4**(3), pp. 193–218.
[6] Williams, F. A., 1985, *Turbulent Combustion*, SIAM, Philadelphia, PA.
[7] Peters, N., 1999, "The Turbulent Burning Velocity for Large Scale and Small Scale Turbulence," J. Fluid Mech., **384**, pp. 107–132.
[8] Tan, Z., 2003, "Multi-Dimensional Modeling of Ignition and Combustion in Premixed and DIS/CI (Direct Injection Spark/Compression Ignition) Engines," Ph.D. thesis, University of Wisconsin-Madison, Madison, WI.
[9] Curran, H. J., Gaffuri, P., Pitz, W. J., and Westbrook, C. K., 2002, "A Comprehensive Modeling Study of Iso-Octane Oxidation," Combust. Flame, **129**(3), pp. 253–280.
[10] Liang, L., 2006, "Multidimensional Modeling of Combustion and Knock in Spark-Ignition Engines With Detailed Chemical Kinetics," Ph.D. thesis, University of Wisconsin-Madison, Madison, WI.
[11] Yang, S., Reitz, R. D., Iyer, C. O., and Yi, J., 2008, "Improvements to Combustion Models for Modeling Spark-Ignition Engines Using the G-Equation and Detailed Chemical Kinetics, SAE Paper No. 2008-01-1634.
[12] Yang, S., Reitz, R. D., Iyer, C. O., and Yi, J., 2008, "A Transport Equation Residual Model Incorporating Refined G-Equation and Detailed Chemical Kinetics Combustion Models," SAE Paper No. 2008-01-2391.
[13] S. Yang and R. D. Reitz, 2009, "Integration of a Continuous Multi-Component Fuel Evaporation Model With an Improved G-Equation Combustion and Detailed Chemical Kinetics Model With Application to GDI Engines," SAE Paper No. 2009-01-0722.
[14] Chou, G. F., and Prausnitz, J. M., 1986, "Adiabatic Flash Calculations for Continuous or Semi-Continuous Mixtures Using an Equation of State," Fluid Phase Equilib., **30**, pp. 75–82.
[15] Han, Z., and Reitz, R. D., 1995, "Turbulence Modeling of Internal Combustion Engines Using RNG κ-ε Models," Combust. Sci. Technol., **106**, pp. 267–295.
[16] Rose, J. W., and Cooper, J. R., 1977, *Technical Data on Fuel*, Wiley, New York.
[17] Kalghatgi, G. T., 2005, "Auto-Ignition Quality of Practical Fuels and Implications for Fuel Requirements of Future SI and HCCI Engines," SAE Paper No. 2005-01-0239.